

ORIGINAL RESEARCH PAPER

Mechanical Integrity Reduction in the Polymeric-pulsatile-pressurized Vessel under Strain-induced Degradation Model

M. Kazemian, A. Hassani*, A. Moazemi Goudarzi

Department of Mechanical Engineering, Babol Noshirvani University of Technology, Babol, Iran.

Article info

Article history:

Received 06 May 2021
Received in revised form
20 August 2021
Accepted 25 August 2021

Keywords:

Polymeric degradable vessel
Pure mechanical degradation
Pulsatile pressure
Finite deformation
Finite element method

Abstract

This paper studies the mechanical behavior of a polymeric degradable vessel subjected to internal pulsatile pressure, external pressure, and axial elongation. Two deformation-induced evolution laws are selected to investigate time-position-dependent material properties of the polymeric vessel. The vessel is subjected to the neo-Hookean constitutive model and an axisymmetric condition. To simulate finite deformation in the degradable vessel, FlexPDE commercial software is invoked in which the governing equations are solved by Standard Galerkin Finite Element Method (SGFEM). Results show that stresses pulsationally increase during degradation. Deformation response of the degradable vessel against time reveals the creep-like behavior of degradable polymers. Degradation rate begins from an initial peak value and decreases over time. The impact of degradation on invariants of the deformation tensor versus time and the vessel radius is discussed. Degradation evolution is higher in the outer radius of the vessel because of higher deformation in this region.

Nomenclature

a	Stent inner radius	\mathbf{B}	Left Cauchy-Green deformation tensor
b	Stent outer radius	\mathbf{C}	Right Cauchy-Green deformation tensor
D	Driving force	D_0	Threshold of degradation
D_1	Degradation rate coefficient	d	Degradation field
\mathbf{F}	Deformation gradient	\mathbf{I}	Identity tensor tensor
J	Volume ratio	K	Bulk modulus
L	Stent length	n	Rate sensitivity index
p	Response to incompressibility	R	Inner radius of artery
R_i	Internal radius of stent	\mathbf{T}	Cauchy stress tensor
\mathbf{T}_0	First Piola-Kirchhoff stress	t_a	Artery wall thickness
t_b	Wall thickness behind the core	t_c	Fibrous cap thickness
t_s	Thickness of the stent	u_R	Lagrangian radial displacement
u_Z	Lagrangian axial displacement	β	Degradation constant
Γ	Degradation constant	ν	Poisson ratio

*Corresponding author: A. Hassani (Assistant Professor)
E-mail address: hassani@nit.ac.ir
<http://dx.doi.org/10.22084/jrstan.2021.24543.1181>
ISSN: 2588-2597

I_1	First invariant of right Cauchy-Green deformation tensor	I_2	Second invariant of right Cauchy-Green deformation tensor
μ	Shear modulus	$\psi(J)$	Volumetric portion of Helmholtz energy function

1. Introduction

Biomaterials are used in biological systems to assess, treat, enhance, or repair any body tissue or organ. When the materials are applied during a given time, at which they should be eliminated as soon as the desired effect is reached, biodegradable materials can be used. Take, for example, stents, bone scaffolds, suture, screw and platinum of orthopedics, and dental implants, which are used in the medical industry [1, 2, and 3].

Polymers are one of the most widely used materials in biodegradable applications due to their appropriate physical and chemical properties in a gradual degradation manner [4]. The loss of mechanical integrity due to exposure to external factors, such as thermal stimuli, and mechanical loads, leads to polymer degradations. Due to the low rate of degradation, the aggressive material finds enough time to penetrate into the volume of degradable polymers, so degradation in the polymers often occurs in its bulk type. In fact, as the overall profile of the body is maintained, the mechanical integrity of the polymer reduces due to chain scissions [5 and 6].

Some of the challenges to experimenting with biodegradable materials are the danger of in-vivo experiments, expensive costs, and the need for advanced empirical techniques. As a result, many efforts have been made to introduce appropriate constitutive models to predict the behavior of biodegradable materials [7]. In recent years, many constitutive models have been proposed to analyze degradation in various case studies, such as interactions between biodegradable stents and blood flow [8 and 9] as well as between bones and biodegradable bone scaffolds [10 and 11]. According to the logic used in the development of evolution laws, they can be classified into two types: physical and phenomenological approaches [8].

The physical approach applies the fundamental principles to derive the constitutive equations, whereas the phenomenological approach empirically relates an observed phenomenon to its cause without paying detailed attention to its fundamental significance [12]. The transient diffusion-reaction model with the physical approach to Poly (L-lactic acid)-covered stents was presented by Prabhu and Hassaini [13] which was based on four characteristics: polymer transfer rate, water molecules, oligomers, and lactic acid coatings. Shazly et al. [14] proposed a physical model of the polymeric stent in which the transient diffusion-reaction equations were separately defined for each

bond of the polymer as a function of hydrolysis, the effect of autocatalysis, and stoichiometric coefficients. Luo et al. [15] introduced a phenomenological model for a polymeric stent based on experimental observation. In this model, the degradation equation was a function of strain, time, and five experimental constants.

Studies on mechanically induced degradation of polymers based on the principles of thermodynamics which implemented according to the phenomenological approach are significant. A phenomenological model for polymers was derived by Rajagopal et al. [16] based on the laws of thermodynamics, in which strain was considered the only source of dissipation. The energy function was dependent upon deformation, and a scalar field was assumed to be equivalent to the degree of degradation. The dissipation rate was explicitly a function of degradation. Soares et al. [17] introduced the nonlinear behavior of polymers with a hyperelastic constitutive model and provided a phenomenological model for degradation. In this model, like Rajagopal, a degradation parameter was used to simulate the reduction in material properties. Degradation field was dependent on the invariants of the Right Cauchy-Green deformation tensor. In the Khan and El-Sayed model [18], similar to that of Soares, the degradation equation was phenomenologically defined, and degradation was assumed to be equivalent to the reduction in mechanical properties of the material. Nonlinear polymeric behavior with large deformations was captured by the Ogden-type hyper-viscoelastic model.

This paper studies a different computational model from what was studied in [16, 17, and 18]. To study degradation accurately and quantitatively in practical applications, especially in medical cases, more aspects and more real constants should be considered. However, to make the computational model more practical, the present study qualitatively investigates the mechanical behavior of a vessel subjected to deformation-induced inhomogeneous-degradation in the coronary artery. Two phenomenologically based degradation models, i.e. Rajagopal et al. [16] and Soares et al. [17] are selected to simulate time-position-dependent material properties of the vessel. The vessel is assumed to include internal pulsatile pressure, external pressure due to plaque, and axial elongation. The constitutive model is considered to be neo-Hookean, and the vessel is assumed to be an axisymmetric model. To solve governing equations of the degradable vessel, SGFEM is used. This method is also verified against the analytical solution to a simple shear case under degradation.

2. Degradation Models

In this paper, Rajagopal et al. [16] and Soares et al. [17] evolution laws are selected as the degradation models. Both of the models are provided based on the phenomenological approach as it would allow to study the degradation process without using concepts of the microscopic phenomenon. This is implemented by defining an internal variable, a scalar field which is termed as the degree of degradation, in the Helmholtz energy function (or free-energy function) of neo-Hookean hyperelastic material model. When the degradation process proceeds, the mechanical properties of the polymer and its capacity to store energy reduce. Therefore, in addition to deformation, the free-energy function is also dependent on degradation. In the following, the fundamental equations governing the two degradable models are presented, however, more details of the two models can be observed in [16 and 17].

2.1. Rajagopal Model

The model [16] is based on thermodynamic principles expressing the response of polymeric material to degradation, known as chain scissions, through the dissipative energy concepts. The only source of dissipative energy is assumed to be strain. $d = d(x, t)$ denotes the degree of local degradation at a given particle located at position x and at time t . $d = 0$ represents the virgin specimen, and $d = 1$ corresponds to the state of maximum possible degradation. According to the model, the elastic response of the material is similar to neo-Hookean model if the amount of degradation is constant. The shear modulus decreases while degradation increases, so:

$$\mu(d) = \mu_0(1 - \beta d), \quad (1)$$

in which μ_0 is the initial shear modulus of the virgin body, and $\beta \leq 1$ is a constant. If $\beta = 1$, the failure continues until full degradation.

The process of polymer degradation is considered to be quasi-static because of the low degradation rate [16 and 17]. As a result, the equilibrium equation in the absence of the body force is:

$$\text{div}(\mathbf{T}) = 0 \quad (2)$$

where \mathbf{T} is Cauchy stress tensor:

$$\mathbf{T} = p\mathbf{1} + \mu(d)\mathbf{B}, \quad \mathbf{B} = \mathbf{F}\mathbf{F}^T, \quad (3)$$

p , \mathbf{F} , \mathbf{B} , and $\mathbf{1}$ are material response to incompressibility, the deformation gradient, left Cauchy-Green deformation tensor, and identity tensor, respectively.

The evolution law is:

$$\frac{\partial d}{\partial t} = \left\{ \frac{D - D_0}{D_1} \right\}^n (1 - d) \quad \text{if } D \geq D_0, \quad (4)$$

where D , D_0 , D_1 , and n are the driving force, threshold of degradation, degradation rate coefficient, and rate sensitivity index, respectively.

The driving force D is defined as a restriction to the degradation process, so degradation occurs when the amount of driving force reaches the threshold required to start degradation in the material. The driving force depends on \mathbf{F} through the first invariant of the Right Cauchy-Green deformation tensor:

$$D = \frac{1}{2}\beta\mu_0(I_1 - 3) \geq 0, \quad I_1 = \text{tr}(\mathbf{F}^T\mathbf{F}) = \text{tr}(\mathbf{C}) \quad (5)$$

in which \mathbf{C} is right Cauchy-Green deformation tensor, and I_1 is its first invariant.

Eqs. (2) and (4) regarding the constitutive Eq. (3) are the fundamental relations governing the Rajagopal degradation model.

2.2. Soares Model

In this model [17], similar to [16], $d = d(x, t)$ is the degradation parameter. Shear modulus during the degradation process changes as [17]:

$$\mu = \mu_0(1 - d). \quad (6)$$

The stress-strain relation obeys the neo-Hookean constitutive model following Eq. (3). The degradation rate is defined as:

$$\begin{aligned} \frac{\partial d}{\partial t} &= \Gamma(1 - d)[(I_1 - 3)^2 + (I_2 - 3)^2]^{1/2}, \\ I_2 &= \frac{1}{2}[(\text{tr}(\mathbf{C}))^2 - \text{tr}(\mathbf{C}^2)] \end{aligned} \quad (7)$$

where Γ is the constant associated with material properties, and I_2 is the second invariant of right Cauchy-Green deformation tensor. If there is no deformation, $I_1 = I_2 = 3$, no degradation occurs [17].

Equilibrium Eq. (2) and evolution Eq. (7) are the governing equations in the Soares degradation model.

3. The Polymeric Degradable Vessel under Inflation and Extension

Based on two introduced models, a polymeric vessel with conditions similar to stents in the coronary artery subjected to the internal pressure on the inner edge, external pressure on the outer edge, and extensional deformation is simulated. The vessel is modeled as an axisymmetric thick-walled cylinder. The loadings are chosen in a way that the degradation parameter is dependent on both position and time. The percentage of arterial stenosis decreases through stent expansion and thereby causes compression in the plaque.

3.1. Inner Pressure Condition

The inner pressure of the vessel is influenced by pulsatile blood pressure that changes in a cardiac cycle as Fig. 1 [19].

3.2. Outer Pressure Condition

To determine the outer pressure, an axisymmetric model including artery, plaque, and stent, is simulated in ANSYS based on the schematic model presented in Fig. 2. In this model, in the initial state, 66% of the artery lumen is blocked by the plaque and falls to 30% by stent inflation when imposing radial displacement. The radial stress imposed on the artery (fibrous cap) is assumed to be the constant outer pressure of the vessel. In Fig. 2, the inner radius of the artery $R = 1.5\text{mm}$, artery wall thickness $t_a = 0.5\text{mm}$, wall thickness behind the core $t_b = 100\mu\text{m}$, and fibrous cap thickness $t_c = 60\mu\text{m}$ are defined [20, 21 and 22].

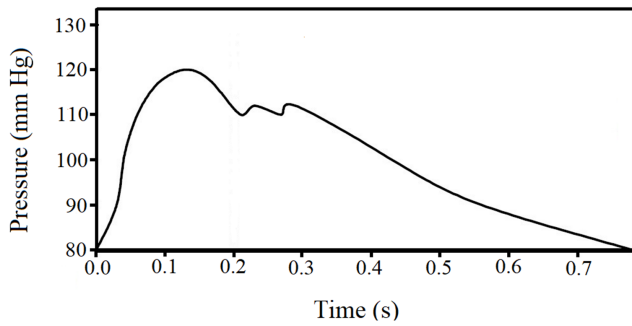


Fig. 1. Inlet pulsatile blood pressure pattern [19].

The plaque profile is modeled as a diffuse shape, reported as one of the typical coronary plaque in relevant references [and]. The length of plaque is assumed to be $1.3R$. The stent is modeled as a circular cylinder. The internal radius and thickness of the stent are $R_i = 0.3\text{mm}$ and $t_s = 0.2\text{mm}$, respectively. The length of the stent is assumed to be $2R$. The elastic modulus of the artery and fibrous cap, with the same materials, are considered to be 1500kPa [25]. The shear modulus of the polymeric stent is selected to be $\mu = 1\text{GPa}$ [26 and 17]. The plaque core is mainly composed of lipid, a very soft tissue of the elastic modulus 10kPa [27 and 22]. Since a significant part of human body tissue is composed of water, the live tissue tends to be incompressible. Therefore, the Poisson ratio $\nu = 0.499$ is used for polymeric stent, artery, and plaque components [25, 28 and 29].

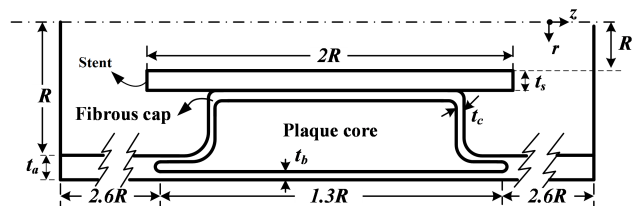


Fig. 2. Dimension of artery, plaque, and stent.

According to the dimensions defined for the model, the stent is inflated to move 0.55mm in radius direction and consequently artery stenosis reduces from 66% to 30%. The bottom edge of the stent is fixed in the axial direction (z direction) and the slide of the stent on the artery is allowed so that there would be no friction between the stent and artery. The radial stress of the fibrous cap is presented in Fig. 3. As can be seen, the radial stress of the artery is 206kPa in magnitude. Therefore, the pressure 206kPa is applied as the constant external pressure of the stent.

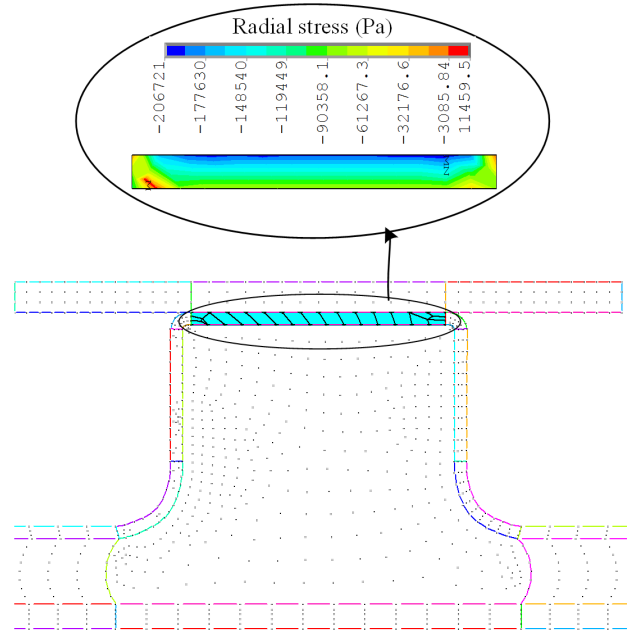


Fig. 3. Radial stress distribution on artery.

3.3. Degradable Vessel

The vessel with the geometry and material properties presented in the previous section is subjected to boundary conditions as Fig. 4. The bottom edge is fixed in z direction and the top edge is under an extension of 0.3mm . The inner and outer radii of the vessel are exposed to the internal pulsatile pressure [19] and constant external pressure 206kPa , respectively. The degradation of the vessel is predicted by Soares and Rajagopal models where degradation constants are assumed to be $n = 1$, $D_1 = 4e6 \times \mu$, $D_0 = 0\text{Pa}$, $\beta = 1$, and $\Gamma = 7e - 6$.

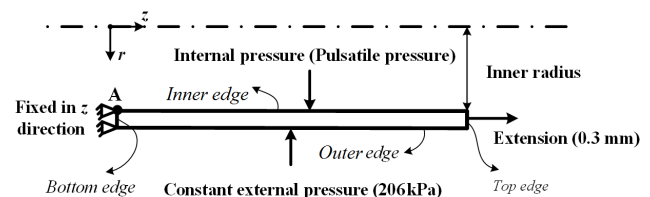


Fig. 4. Boundary conditions for the biodegradable vessel.

3.4. Governing Equations

Regarding the axisymmetric and plane strain conditions, displacement field of the degradable vessel in the Lagrangian description is expressed as:

$$u_r = u_R(R, Z, t), \quad u_\theta = 0, \quad u_z = u_Z(R, Z, t), \quad (8)$$

where $a \leq R \leq b$ and $0 \leq Z \leq L$ are the undeformed radius and length, respectively. Here, a , b , and L denote inner and outer radii and the vessel length, each. The deformation gradient \mathbf{F} , left Cauchy-Green deformation tensor \mathbf{B} , and right Cauchy-Green deformation tensor \mathbf{C} can be described as [12]:

$$\mathbf{F} = \mathbf{I} + \nabla \mathbf{u}, \quad \mathbf{B} = \mathbf{F}\mathbf{F}^T, \quad \mathbf{C} = \mathbf{F}^T\mathbf{F} \quad (9)$$

Regarding the displacement field, \mathbf{F} is:

$$\mathbf{F} = \begin{bmatrix} 1 + \frac{\partial u_R(R, Z, t)}{\partial R} & 0 & \frac{\partial u_R(R, Z, t)}{\partial Z} \\ 0 & 1 + \frac{u_R(R, Z, t)}{R} & 0 \\ \frac{\partial u_Z(R, Z, t)}{\partial R} & 0 & 1 + \frac{\partial u_Z(R, Z, t)}{\partial Z} \end{bmatrix} \quad (10)$$

accordingly, the components of \mathbf{B} and \mathbf{C} reach:

$$B_{RR} = \left(1 + \frac{\partial u_R(R, Z, t)}{\partial R}\right)^2 + \left(\frac{\partial u_R(R, Z, t)}{\partial Z}\right)^2,$$

$$B_{ZZ} = \left(1 + \frac{\partial u_Z(R, Z, t)}{\partial Z}\right)^2 + \left(\frac{\partial u_Z(R, Z, t)}{\partial R}\right)^2,$$

$$C_{\theta\theta} = B_{\theta\theta} = \left(1 + \frac{u_R(R, Z, t)}{R}\right)^2,$$

$$C_{RR} = \left(1 + \frac{\partial u_R(R, Z, t)}{\partial R}\right)^2 + \left(\frac{\partial u_Z(R, Z, t)}{\partial R}\right)^2,$$

$$C_{ZZ} = \left(1 + \frac{\partial u_Z(R, Z, t)}{\partial Z}\right)^2 + \left(\frac{\partial u_R(R, Z, t)}{\partial Z}\right)^2,$$

$$B_{RZ} = B_{ZR} = \left(1 + \frac{\partial u_R(R, Z, t)}{\partial R}\right) \left(\frac{\partial u_Z(R, Z, t)}{\partial R}\right), \\ + \left(1 + \frac{\partial u_Z(R, Z, t)}{\partial Z}\right) \left(\frac{\partial u_R(R, Z, t)}{\partial Z}\right),$$

$$C_{RZ} = C_{ZR} = \left(1 + \frac{\partial u_R(R, Z, t)}{\partial R}\right) \left(\frac{\partial u_R(R, Z, t)}{\partial Z}\right), \\ + \left(1 + \frac{\partial u_Z(R, Z, t)}{\partial Z}\right) \left(\frac{\partial u_Z(R, Z, t)}{\partial R}\right),$$

$$B_{R\theta} = B_{\theta R} = C_{R\theta} = B_{Z\theta} = B_{\theta Z} = C_{Z\theta} = C_{\theta Z} = 0 \quad (11)$$

According to Eqs. (4), (5), and (11) Rajagopal' evolution law is:

$$\frac{Dd}{Dt} = \left\{ \frac{D - D_0}{D_1} \right\}^n (1 - d),$$

$$D = \frac{1}{2}\beta\mu_0 \left\{ \left(1 + \frac{\partial u_R(R, Z, t)}{\partial R}\right)^2 + \left(\frac{\partial u_Z(R, Z, t)}{\partial R}\right)^2 \right. \\ \left. + \left(1 + \frac{u_R(R, Z, t)}{R}\right)^2 + \left(1 + \frac{\partial u_Z(R, Z, t)}{\partial Z}\right)^2 \right. \\ \left. + \left(\frac{\partial u_R(R, Z, t)}{\partial Z}\right)^2 - 3 \right\} \quad (12)$$

where, $\frac{D(\cdot)}{Dt}$ denotes material time derivative.

The degradation rate of Soares's model is determined by Eq. (7) and (11):

$$\frac{Dd}{Dt} = \Gamma(1 - d) [(I_1 - 3)^2 + (I_2 - 3)^2]^{\frac{1}{2}},$$

$$I_1 = \left(1 + \frac{\partial u_R(R, Z, t)}{\partial R}\right)^2 + \left(\frac{\partial u_Z(R, Z, t)}{\partial R}\right)^2$$

$$+ \left(1 + \frac{\partial u_Z(R, Z, t)}{\partial Z}\right)^2 + \left(1 + \frac{\partial u_R(R, Z, t)}{R}\right)^2 \\ + \left(\frac{\partial u_R(R, Z, t)}{\partial Z}\right)^2,$$

$$I_2 = \frac{I_1}{2} - \frac{1}{2} \left\{ \left[\left(1 + \frac{\partial u_R(R, Z, t)}{\partial R}\right) \left(\frac{\partial u_R(R, Z, t)}{\partial Z}\right) \right. \right.$$

$$\left. + \left(1 + \frac{\partial u_Z(R, Z, t)}{\partial Z}\right) \left(\frac{\partial u_Z(R, Z, t)}{\partial R}\right) \right]^2$$

$$+ \left[\left(1 + \frac{\partial u_R(R, Z, t)}{\partial R}\right)^2 + \left(\frac{\partial u_Z(R, Z, t)}{\partial R}\right)^2 \right]^2$$

$$+ \left[\left(1 + \frac{\partial u_Z(R, Z, t)}{\partial Z}\right)^2 + \left(\frac{\partial u_R(R, Z, t)}{\partial Z}\right)^2 \right]^2$$

$$+ \left[\left(1 + \frac{\partial u_R(R, Z, t)}{\partial R}\right) \left(\frac{\partial u_R(R, Z, t)}{\partial Z}\right) \right.$$

$$\left. + \left(1 + \frac{\partial u_Z(R, Z, t)}{\partial Z}\right) \left(\frac{\partial u_Z(R, Z, t)}{\partial R}\right) \right]^2$$

$$+ \left(1 + \frac{\partial u_R(R, Z, t)}{\partial R}\right)^4 \left. \right\}.$$

(13)

According to volume ratio J , the determinant of \mathbf{F} , Cauchy's stress in Eq. (3) can be converted to the first

Piola-Kirchhoff stress [12]:

$$\begin{aligned} \mathbf{T}_0 &= J\mathbf{T}\mathbf{F}^{-T}, \\ J &= \frac{R + u_R(R, Z, t)}{R} \left[\frac{\partial u_R(R, Z, t)}{\partial R} \frac{\partial u_z(R, Z, t)}{\partial Z} \right. \\ &\quad - \frac{\partial u_z(R, Z, t)}{\partial R} \frac{\partial u_R(R, Z, t)}{\partial Z} \\ &\quad \left. + \frac{\partial u_R(R, Z, t)}{\partial R} + \frac{\partial u_z(R, Z, t)}{\partial Z} + 1 \right]. \end{aligned} \quad (14)$$

Considering constitutive relation (3) and the components of \mathbf{F} and \mathbf{B} in Eqs. (10) and (11), the equilibrium equations in the cylindrical annular region can be obtained regarding the Lagrangian description:

$$\begin{aligned} &\frac{\partial}{\partial R} [JF_{RR}^{-T}(pI + \mu_0(1 - \beta d)B_{RR})] \\ &+ \frac{1}{R} [(1 - \beta d)J\mu_0(F_{RR}^{-T}B_{RR} - F_{\theta\theta}^{-T}B_{\theta\theta}) \\ &+ PIJ(F_{RR}^{-T} - F_{\theta\theta}^{-T})] + \frac{\partial}{\partial Z} [JF_{RZ}^{-T}\mu_0(1 - \beta d)B_{RZ}] = 0, \\ &\frac{\partial}{\partial R} [JF_{RZ}^{-T}\mu_0(1 - \beta d)B_{RZ}] + \frac{\partial}{\partial Z} [JF_{ZZ}^{-T} + \mu_0(pI \\ &+ \mu_0(1 - \beta d)B_{ZZ})] + \frac{1}{R} [JF_{RZ}^{-T}\mu_0(1 - \beta d)B_{RZ}] = 0. \end{aligned} \quad (15)$$

Regarding Fig. 4, the inner radius is exposed to the pulsatile pressure P^{puls} :

$$T_{rr}(a, Z, t) = -P^{puls}, \quad \text{for } \forall t \geq 0 \text{ and } Z \in (0, L) \quad (16)$$

The outer boundary is assumed to be the plaque pressure $P^{plaque} = -206\text{KPa}$:

$$T_{rr}(b, Z, t) = P^{plaque}, \quad \text{for } \forall t \geq 0 \text{ and } Z \in (0, L) \quad (17)$$

The boundary conditions in terms of axial displacement are considered as:

$$\begin{aligned} u_z(R, 0, t) &= 0, \quad u_z(R, L, t) = 0.3\text{mm}, \\ &\text{for } \forall t \geq 0 \text{ and } R \in (a, b). \end{aligned} \quad (18)$$

The initial condition governing the degradation field is:

$$d(R, Z, 0) = 0, \quad \text{for } R \in (a, b) \text{ and } Z \in (0, L). \quad (19)$$

It is worth mentioning that in the initial state, the vessel properties are virgin, $d = 0 \rightarrow \mu = \mu_0$, so the degradable vessel responds as the neo-Hookean material model with intact shear modulus.

The constitutive equation for p is defined as [12]:

$$p(R, Z, t) = \frac{d\psi(J)}{dJ} = K(J - 1), \quad (20)$$

in which $\psi(J)$ and K are the volumetric portion of Helmholtz energy function and bulk modulus, respectively. This relation is commonly used in the volumetric portion of free-energy functions being in a decoupled form, such as the neo-Hookean incompressible material model, to impose incompressibility and calculate p [12 and 31].

Consequently, evolution law (12) for the Rajagopal model (or (13) for the Soares model) and two equilibrium relations (15) can be solved to reach the displacement fields $u_R(R, Z, t)$ and $u_z(R, Z, t)$ and degradation parameter $d(R, Z, t)$. Regarding Eq. (20), the material response to incompressibility $p(R, Z, t)$ depends on the displacement fields.

4. Standard Galerkin Finite Element Method (SGFEM) Through FlexPDE Software

The degradation problem is of a transient one in which material properties vary during the process in terms of time and position. This can limit the degradation analysis in finite element software, for example, in ANSYS there are general challenges in the execution of this problem. First, it is impossible to update element properties during a transient solution, and the second is that the evolution equation could not be applied as an additional governing equation to the fundamental equations of the element [30 and 31]. Thus, there is no alternative unless programming in APDL (ANSYS parametric design language) [30 and 31].

To analyze the defined degradable vessel, this paper uses FlexPDE commercial software. It allows the user to apply differential equations to describe the system in its programming environment in which the script language is of a natural type [32]. The governing equations are solved by SGFEM and the results are presented as graphs, contours, and data [32]. The software does not have element libraries and the solution is found by defining the governing equations, and imposing boundary and initial conditions on the computational domain [32]. Regarding Fig. 5, the solution algorithm of FlexPDE according to SGFEM is as follows [31-33]:

1. The weighted-residual statements of all differential equations are established.
2. The interpolation functions are invoked, and by integrating over the element, the matrices of standard Galerkin method are derived.
3. The assembled matrices of the problem are developed.
4. The final algebraic equations are solved by the Newton-Raphson method through an implicit backward difference approach.

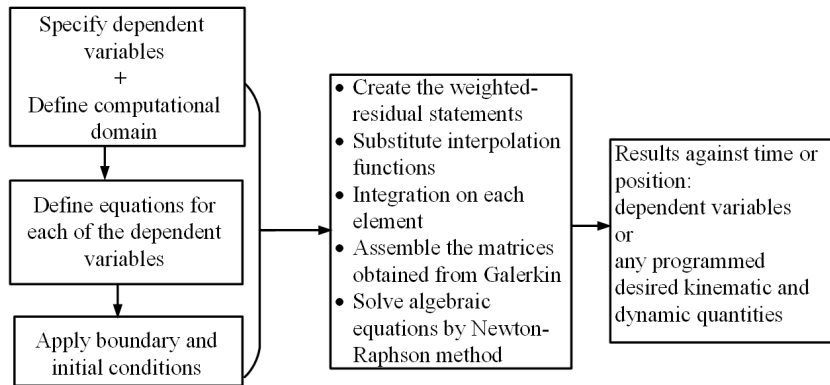


Fig. 5. The solution process in FlexPDE software according to SGFEM.

The components of displacement and degradation parameter d are considered the degrees of freedom chosen in the finite element procedure. The governing differential equations associated with components of displacement and degradation parameter d are defined by their corresponding equilibrium relations and the evolution law in Eqs. (15) and (12) (or (13)), respectively.

5. Results and Discussions

The main purpose of the present work is to study some mechanical components of the degradable vessel but not to discuss which model is more successful in predicting degradation process of biodegradable stent. According to the assumed degradation parameters in section 3.3, the degradation process of stent proceeds about $1e7$ cardiac cycles or about three months.

Fig. 6 compares the degradation parameter of Rajagopal and Soares at the material point initially located at the inner radius of 0.3mm (point A) during $1e7$ cardiac cycles. A higher level of degradation occurs in the Rajagopal model than in the Soares model. Owing to the equality of material properties and the constitutive equations of the two models in the initial state, different degradation rates are dependent only on the evolution laws and parameters existing in them. Fig. 7 indicates the degradation rate at point A. As expected, there is a higher rate of degradation in the Rajagopal stent than in the Soares stent. A higher rate of degradation results in a greater amount of degradation in Rajagopal vessel at a given time interval. During the degradation process, over time, the number of bonds and subsequently the rate of degradation decreases. In other words, the ability of body to degrade decreases. This causes the rate of degradation to reduce, Fig. 7.

Fig. 8 shows degradation at the bottom edge of the stents calculated in the third month, i.e. at the end of $1e7$ cardiac cycles. It indicates an increase in the amount of degradation versus the radius of Rajagopal and Soares vessels. The theory of the two proposed degradation models is based on the distributed strain in body. In other words, the higher the deformation,

the higher the level of degradation.

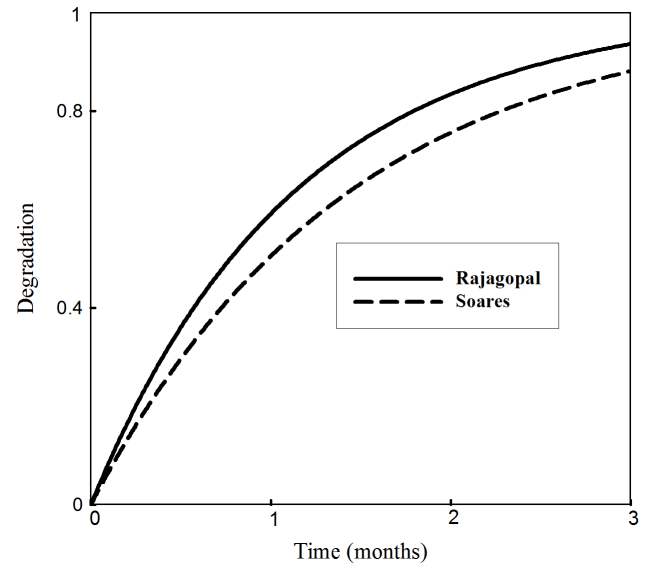


Fig. 6. Degradation evolution at point A in the vessels during $1e7$ cardiac cycles.

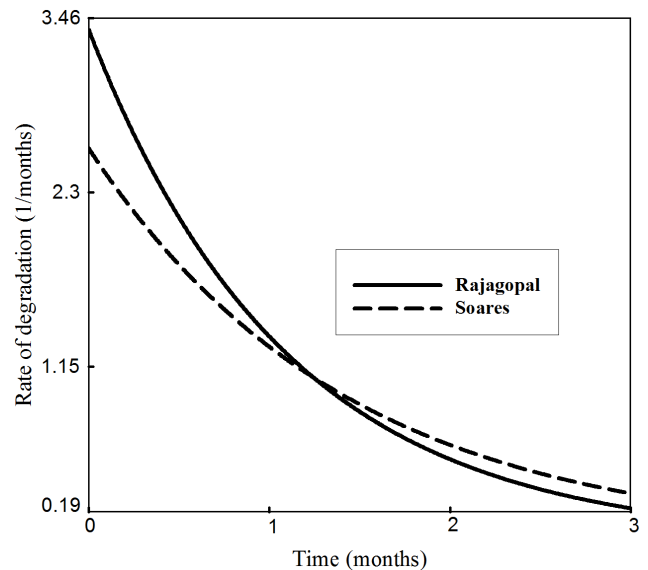


Fig. 7. The degradation rates of two vessels at point A during $1e7$ cardiac cycles.

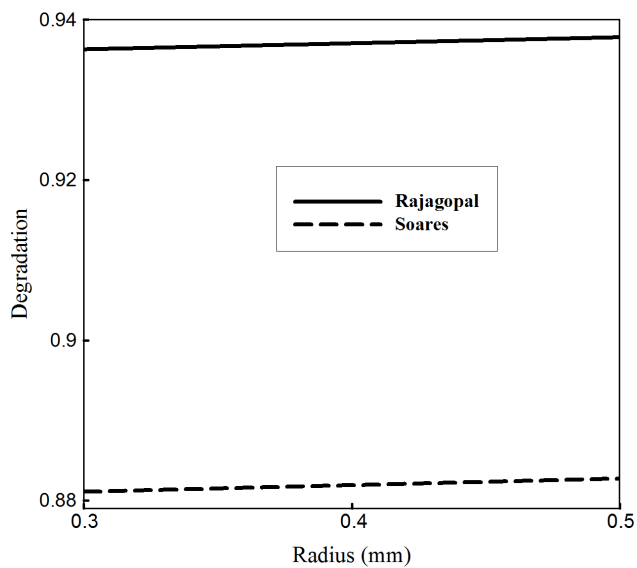


Fig. 8. Degradation at the bottom edge of vessels against radius in the third month.

As the evolution equations of two models show, the strain effect on degradation can be expressed by either merely the first invariant of \mathbf{C} or both the first and the second invariants of \mathbf{C} . The former is related to the Rajagopal model, whereas the latter is associated with the Soares model. Therefore, at a given position of body where the values of these invariants are higher, degradation is also greater.

For a more comprehensive investigation, at the bottom edge, the first and the second invariants of \mathbf{C} versus the radius of Rajagopal and Soares vessels at the end of $1e7$ cardiac cycles are studied, Fig. 9. An upward trend can be seen in the values of the invariants from the inner edge to the outer edge. This means that the deformation is higher at the outer radius of two degradable polymeric stents because the external pressure on them is greater than the internal pressure. The invariants at the material point A versus time during $1e7$ cardiac periods are also illustrated in Fig. 10. As can be seen, the invariants grow over time, indicating a creep-like behavior in the polymer degradation process. This is due to material softening over time, which is induced by degradation [16, 17, and 31]. The increase and decrease in strain tensor in the 2D and 3D models could be measured by invariants of \mathbf{C} ; the more invariants, the more strain. Clearly, the strain in Rajagopal and Soares degradable vessels increases with the passage of time.

In order to investigate the effect of degradation on the vessel stress, the hoop and radial stresses are calculated at the inner radius of Rajagopal vessel at point A against twenty cardiac cycles in Fig. 11a and Fig. 11b, respectively. Due to the fact that the vessel is exposed to greater pressure in the outer radius than the inner radius, the two stresses show a negative value. The absolute value of hoop stress rises during degradation

compared to its initial state because of degradation-induced material softening. The stress promotion in the degradable vessels under time-independent applied pressure can be also found in [31, 34, 35 and 36]. Here, considering the cyclic pressure on the inner radius of degradable vessel, which alone leads to the positive hoop stress, the stress increases with a pulsatile profile like the pressure presented in Fig. 1. According to the assumed boundary condition (16), the radial stress due to the pulsatile pressure is negative, so the radial stress behaves as the convex type of the applied time-dependent pressure on the vessel, being constant compared to previous cycles. The maximum error in predicting the radial stress calculated by SGFEM is about 2.5%.

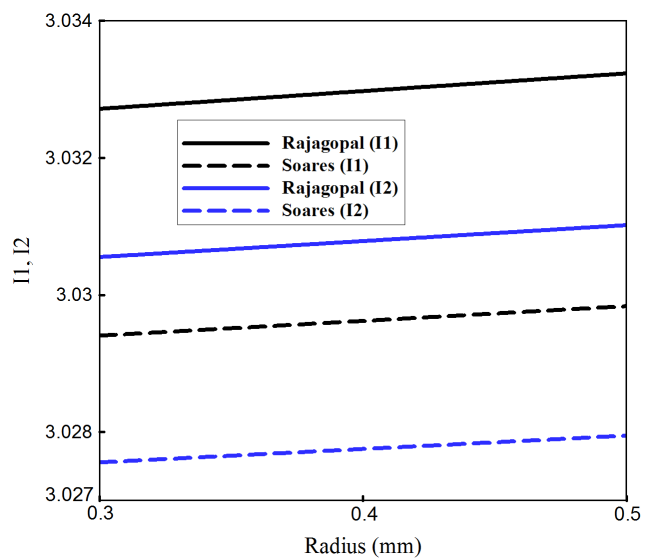


Fig. 9. The first and second invariants of \mathbf{C} at the bottom edge of vessels against radius in the third month.

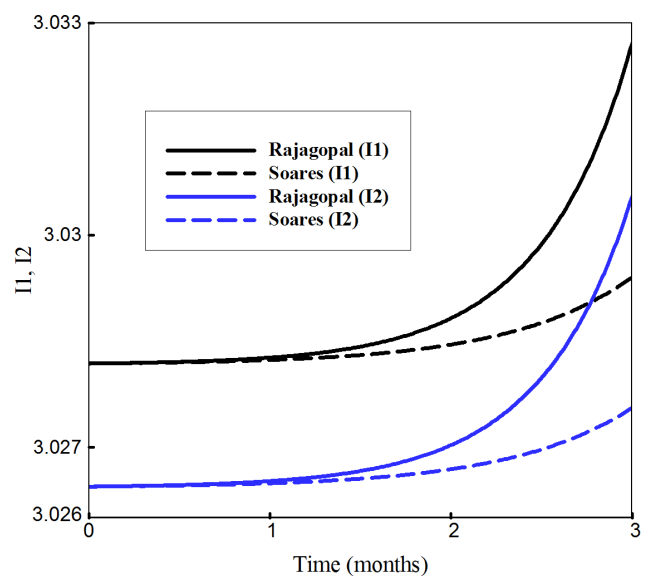


Fig. 10. The first and second invariants of \mathbf{C} versus time at point A during $1e7$ cardiac cycles.

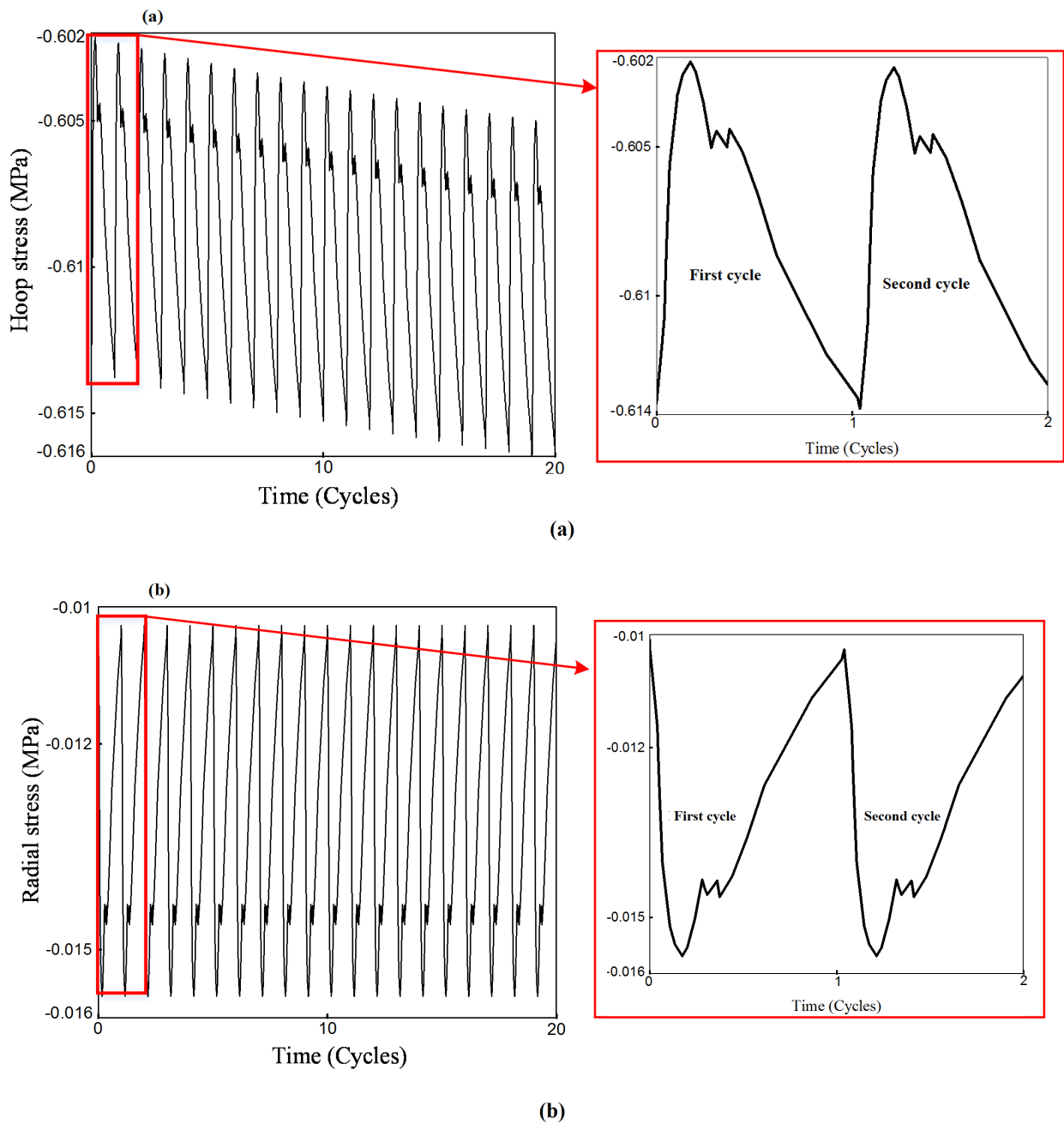


Fig. 11. Evolution of the hoop and radial stresses for the Rajagopal vessel at point A during twenty cardiac cycles in (a) and (b), respectively.

It is worth mentioning that the other quantities, such as degradation and the deformation invariants, also evolve pulsationally but are not noticeable in the presented figures.

6. Conclusions

Two strain-induced bulk degradation models are used to study the mechanical response of a polymeric degradable vessel to the loss of mechanical integrity. The vessel is exposed to pulsatile pressure at the inner radius, constant pressure at the outer radius, and

axial elongation. Evolution equations and their effects on material properties during the degradation process tend to cause a time-position-dependent problem. To solve this, the Standard Galerkin Finite Element Method is applied through FlexPDE commercial software. Given that the vessel is subjected to cyclic pressure, the stress values promote in a pulsatile form against time. The creep-like behavior of the degradable vessel is studied by means of invariants of the deformation tensor. It is shown that the degradation rate is initially maximum but then decreases due to a reduction in the number of polymer chains during degrada-

tion. Owing to higher pressure at outer radius of the degradable vessel, degradation and the first and second invariants of deformation tensor increase in terms of radius.

Conflict of Interest

There is no conflict of interest in this work.

Data Availability

The raw data required to reproduce these findings are available from the corresponding author upon reasonable request.

References

- [1] R. Dwivedi, S. Kumar, R. Pandey, A. Mahajan, D. Nandana, D.S. Katti, D. Mehrotra, Polycaprolactone as biomaterial for bone scaffolds: Review of literature, *J. Oral Biol. Craniofac. Res.*, 10(1) (2020) 381-388.
- [2] H. Lim, S. Ha, M. Bae, S.H. Yoon, A highly robust approach to fabricate the mass-customizable mold of sharp-tipped biodegradable polymer microneedles for drug delivery, *Int. J. Pharm.*, 600 (2021) 120475.
- [3] F. Trentadue, D. De Tommasi, G. Puglisi, A predictive micromechanically-based model for damage and permanent deformations in copolymer sutures, *J. Mech. Behav. Biomed. Mater.*, 115 (2021) 104277.
- [4] F.P. La Mantia, M. Morreale, L. Botta, M.C. Mistretta, M. Ceraulo, R. Scaffaro, Degradation of polymer blends: A brief review, *Polym. Degrad. Stab.*, 145 (2017) 79-92.
- [5] F. von Burkersroda, L. Schedl, A. Göpferich, Why degradable polymers undergo surface erosion or bulk erosion, *Biomaterials*, 23(21) (2002) 4221-4231.
- [6] R. Scaffaro, A. Maio, F. Sutura, E.F. Gulino, M. Morreale, Degradation and recycling of films based on biodegradable polymers: A short review, *Polymers*, 11(4) (2019) 651.
- [7] A.N. Ford Versypt, D.W. Pack, R.D. Braatz, Mathematical modeling of drug delivery from autocatalytically degradable PLGA microspheres - A review, *J. Control. Release*, 165(1) (2013) 29-37.
- [8] E.L. Boland, C.J. Shine, N. Kelly, C.A. Sweeney, P.E. McHugh, A review of material degradation modelling for the analysis and design of bioabsorbable stents, *Ann. Biomed. Eng.*, 44(2) (2016) 341-356.
- [9] T. Pilgrim, M. Rothenbühler, G. CM Siontis, D.E. Kandzari, J.F. Iglesias, M. Asami, T. Lefèvre, R. Piccolo, J. Koolen, S. Saito, T. Slagboom, O. Muller, R. Waksman, S. Windecker, Biodegradable polymer sirolimus-eluting stents vs durable polymer everolimus-eluting stents in patients undergoing percutaneous coronary intervention: A meta-analysis of individual patient data from 5 randomized trials, *Am. Heart J.*, 235 (2021) 140-148.
- [10] Y. Zhang, X. Liu, L. Zeng, J. Zhang, J. Zuo, J. Zou, J. Ding, X. Chen, Polymer fiber scaffolds for bone and cartilage tissue engineering, *Adv. Funct. Mater.*, 29(36) (2019) 1903279.
- [11] L. Gritsch, E. Perrin, J.M. Chenal, Y. Fredholm, A. LB Maçon, J. Chevalier, A. R Boccaccini, Combining bioresorbable polyesters and bioactive glasses: Orthopedic applications of composite implants and bone tissue engineering scaffolds, *Appl. Mater. Today*, 22 (2021) 100923.
- [12] G.A. Holzapfel, *Nonlinear Solid Mechanics: A Continuum Approach for Engineering*. 1th ed. New York: Wiley Editorial Offices, (2000).
- [13] S. Prabhu, S. Hossainy, Modeling of degradation and drug release from a biodegradable stent coating, *J. Biomed. Mater. Res. A*, 80(3) (2007) 732-741.
- [14] T. Shazly, V.B. Kolachalama, J. Ferdous, J.P. Oberhauser, S. Hossainy, E.R. Edelman, Assessment of material by-product fate from bioresorbable vascular scaffolds, *Ann. Biomed. Eng.*, 40(4) (2012) 955-965.
- [15] Q. Luo, X. Liu, Z. Li, C. Huang, W. Zhang, J. Meng, Z. Chang, Z. Hua, Degradation model of bioabsorbable cardiovascular stents, *PLOS ONE*, 9(11) (2014) e110278.
- [16] K.R. Rajagopal, A.R. Srinivasa, A.S. Wineman, On the shear and bending of a degrading polymer beam, *Int. J. Plast.*, 23(9) (2007) 1618-1636.
- [17] J.S. Soares, J.E. Moore Jr., K.R. Rajagopal, Constitutive framework for biodegradable polymers with applications to biodegradable stents, *ASAIO J.*, 54(3) (2008) 295-301.
- [18] K.A. Khan, T. El-Sayed, A phenomenological constitutive model for the nonlinear viscoelastic responses of biodegradable polymers, *Acta Mech.*, 224(2) (2012) 287-305.

- [19] R.M. Berne, M.N. Levy, *Cardiovascular Physiology*. Mosby. St. Louis, (1967) p. 201.
- [20] D.L. Brown, *Cardiovascular Plaque Rupture*. 1th ed. New York: CRC Press, (2002).
- [21] J.C. Wang, S.L.T. Normand, L. Mauri, R.E. Kuntz, Coronary artery spatial distribution of acute myocardial infarction occlusions, *ACC Current Journal Review*, 110(3) (2004) 278-284.
- [22] M. Kazemian, H. Afrasiab, M.H. Pashaei, Comparison of the plaque rupture risk in different double-stenosis arrangements of coronary arteries by modeling fluid-structure interaction, *Modares Mechanical Engineering*, 16(2) (2016) 10-18 (In Persian).
- [23] R. Beaumont, K. Bhaganagar, B. Segee, O. Badak, Using fuzzy logic for morphological classification of IVUS-based plaques in diseased coronary artery in the context of flow-dynamics, *Soft Comput.*, 14 (2010) 265-272.
- [24] K. Bhaganagar, C. Veeramachaneni, C. Moreno, Significance of plaque morphology in modifying flow characteristics in a diseased coronary artery: Numerical simulation using plaque measurements from intravascular ultrasound imaging, *Appl. Math. Model.*, 37(7) (2013) 5381-5393.
- [25] A. Karimi, M. Navidbakhsh, A. Shojaei, S. Faghihi, Measurement of the uniaxial mechanical properties of healthy and atherosclerotic human coronary arteries, *Mater. Sci. Eng. C*, 33(5) (2013) 2550-2554.
- [26] C.M. Agrawal, K.F. Haas, D.A. Leopold, H.G. Clark, Evaluation of poly(L-lactic acid) as a material for intravascular polymeric stents, *Biomaterials*, 13(3) (1992) 176-182.
- [27] A.C. Akyildiz, L. Speelman, H. van Brummelen, M.A. Gutiérrez, R. Virmani, A. van der Lugt, A.F.W. van der Steen, J.J. Wentzel, F.J.H. Gijssen, Effects of intima stiffness and plaque morphology on peak cap stress, *Biomed. Eng. Online*, 10 (2011) 25.
- [28] J.R. Doherty, D.M. Dumont, G.E. Trahey, M.L. Palmeri, Acoustic radiation force impulse imaging of vulnerable plaques: A finite element method parametric analysis, *J. Mech. Eng.*, 46(1) (2013) 83-90.
- [29] M. Kazemian, H. Afrasiab, M.H. Pashaei, R.A. Jafari-Talookolaei, A numerical study based on finite element method on the effect of geometrical parameters of the coronary artery aneurysm on the mechanical stress created on the aneurysm wall, *J. Mech. Eng.*, 50(1) (2020) 181-187.
- [30] ANSYS, Inc., 'ANSYS Help - Release 19', 2018.
- [31] M. Kazemian, A. Moazemi Goudarzi, A. Hassani, A study on an incompressible polymeric pressurized vessel subjected to bulk degradation, *Math. Mech. Solids.*, (2021), DOI:10.1177/10812865211033634.
- [32] FlexPDE 7, PDE Solution Inc., (2017).
- [33] S.M. Ebrahimi, M. Javanmard, M.H. Taheri, M. Barimani, Heat transfer of fourth-grade fluid flow in the plane duct under an externally applied magnetic field with convection on walls, *Int. J. Mech. Sci.*, 128-129 (2017) 564-571.
- [34] M. Kazemian, A. Moazemi Goudarzi, A. Hassani, A Study on Deformation-Induced Degradation of the Compressible Polymeric Pressurized Vessel through a Non-Equilibrium Thermodynamic Framework, *Math. Mech. Solids.*, (2021), DOI:10.1177/10812865211042924.
- [35] J.S. Soares, K.R. Rajagopal, J.E. Moore Jr., Deformation-induced hydrolysis of a degradable polymeric cylindrical annulus, *Biomech. Model. Mechanobiol.*, 9 (2010) 177-186.
- [36] M. Kazemian, A. Hassani, A.M. Goudarzi, On strain-induced degradation of the polymeric skeleton in poro-hyperelastic inflating vessels by a non-equilibrium thermodynamic framework, *Int. J. Eng. Sci.*, 171 (2022) 103618.